Role of crystalline iron oxides on stabilization of inositol phosphates in soil

(Article begins on next page)

28 July 2024

Role of crystalline iron oxides on stabilization of inositol phosphates in soil

Luisella Celi[a], Marco Prati[a], Giuliana Magnacca[b], Veronica Santoro[a*], Maria Martin[a]

[a]DISAFA, Università di Torino, Largo Braccini 2, Grugliasco, Italy

[b]Dipartimento di Chimica, Università di Torino, Via Giuria 7, Torino, Italy

*corresponding author

email address: veronica.santoro@unito.it

Highlights

- Retention of inorganic phosphate and of the organic phosphorus (P) form *myo*-inositol hexaphosphate (InsP6) on four crystalline iron oxides was evaluated

- Reversibility of the reaction was also tested with different extractants

- The capacity of the oxides to retain InsP6 depended on surface properties and stability of the mineral-P complexes

- These factors controlled the reversibility of the reaction and the removal of P from the solids surface

- Stabilization of InsP6 by iron oxides is crucial in controlling P availability and turnover in soils

Abstract

Inositol phosphates selective retention in soil is related to their great affinity to iron (Fe) oxides, with which they interact by the formation of ligand exchange complexes. Soils contain from amorphous to crystalline Fe oxides forms, as goethite (Gt), whose effect on inositol phosphates retention is well-known. The contribution of other widespread crystalline Fe oxides as haematite (Hm), magnetite (Mt) and maghemite (Mh) is instead less known. These oxides display different phosphorus (P) retention and release capacities due to their different surface properties and stability towards protons, organic acids and complexing agents. We therefore investigated: i) the extent and mechanisms of *myo*-inositol hexaphosphate (InsP6) and inorganic phosphate (Pi) adsorption on Gt, Hm, Mt and Mh, also studying the computational geometries of InsP6 molecule; ii) the reversibility of the reaction as affected by pH and in the presence of citrate; iii) the efficiency of NaOH-EDTA on P extraction. Compared to Gt, Hm retained less InsP6, due to the distribution of superficial -OH groups allowing for the interaction of two phosphate groups instead of four, as for Gt. Mt and Mh retained more InsP6 than Hm, also through precipitation processes caused by a partial dissolution of the oxides caused by InsP6. Desorption of InsP6 in the pH range 3.5-8.5 was negligible, except for Hm, while citrate led to larger desorption, with no release from Gt. NaOH-EDTA extraction of InsP6 was instead particularly effective from Gt and less from the other oxides. The four crystalline Fe oxides thus showed different capacity to retain organic P in the form of InsP6 as a function of surface properties and stability of the mineral-P complexes, therefore influencing the extent of release, accumulation and turnover in soils.

Abbreviations: Gt (goethite), Hm (haematite), Mt (magnetite), Mh (maghemite), Pi (inorganic phosphate), InsP6 (*myo*-inositol hexakisphosphate).

Introduction

Inositol phosphates represent the largest organic phosphorus (P) fraction in most soils (Anderson, 1980; George et al., 2018), with concentrations of inositol hexaphosphate ranging between 1 and 460 mg P kg^{-1} (Turner, 2007). The selective accumulation of inositol phosphates has been related, in acidic soils, to their greater affinity for iron (Fe) and aluminium (Al) oxides with respect to P diesters (nucleotides and phospholipids) (Leytem et al. 2002; Gerke 2014). Adsorption on Fe oxide surfaces is favoured by the multiple phosphate groups bound to the inositol moiety that can be attracted by the positive colloidal surface in a large pH range and form a complex by a ligand exchange mechanism (Celi and Barberis, 2004). This interaction is believed to be one of the most important mechanisms for inositol phosphate preservation in soil, due to the great stability of the complex and to the unavailability of the substrate for phytase hydrolysis (George et al., 2005; Giaveno et al., 2010).

Soils can contain various Fe (hydr)oxide forms, differently distributed along the soil profile and/or with soil evolution degree, depending on the complex interaction of time, lithology and climate factors (Cornell and Schwertmann, 1996). Among Fe (hydr)oxides, poorly crystalline forms present a significantly greater P retention capacity compared to crystalline ones (Celi et al., 2003; Yan et al., 2014). Sorption of inositol phosphates increases when (hydr)oxides coprecipitate and/or coat other mineral surfaces, resulting in a larger retention than that estimated by the amount of oxide present in the system (Celi et al., 2003; Santoro et al., 2019). More crystalline (hydr)oxides, such as goethite and haematite, retain inositol phosphates in lower amounts than poorly crystalline (hydr)oxides but with greater stability, which makes the reaction nearly irreversible (Celi et al., 1999; Ognalaga et al., 1994; Yan et al., 2014). However, the relative contribution of other crystalline Fe oxides is poorly known. Iron oxides such as maghemite are also widespread in soils as a product of weathering in well-developed soils. Magnetite is a ferromagnetic mineral containing both Fe^{2+} and Fe^{3+}, mainly present in Oxisols (Schaefer et al., 2008), which can partially or completely oxidize to maghemite (Magnacca et al., 2014). These Fe oxides exhibit marked differences in surface area and distribution of contiguous singly-coordinated hydroxyl groups (Barrón and Torrent, 1996), which are the main properties affecting the specific adsorption of inositol phosphates. In addition, these Fe oxides differ in their

thermodynamic stability and reactivity toward protons, organic acids and complexing agents, such as oxalate, citrate and EDTA (Colombo et al., 1994; Cornell and Schwertmann, 1996), indirectly affecting anion retention. In this context, we should notice that inositol phosphates themselves have a great complexing capacity, favouring a partial dissolution of poorly crystalline Fe (hydr)oxides (Celi et al., 2003). On the other hand, anions such as citrate may compete for surface adsorption sites with adsorbed P (Geelhoed et al., 1998; 1999), changing its bioavailability. Citrate is reported to extract smaller amounts of inositol phosphate with respect to inorganic phosphate (Pi) from goethite (Martin et al., 2004; Yan et al., 2015) and from haematite (Yan et al., 2014), but no information on the other Fe oxides is available.

Thus, in soils characterized by the presence of different Fe forms, the fate of inositol phosphates could not be completely explained based on current knowledge. For instance, McDowell et al. (2007) and Turner et al. (2007) observed that the relative contribution of P-containing compounds to the total organic P varied with soil development in a surprisingly way. In the most developed soils, relatively lower amounts of inositol phosphates and higher percentages of diesters, in particular nucleotides, were indeed extracted. Moreover, a low presence of inositol phosphates has also been reported in places where they should accumulate due to the large amount of Fe and Al (i.e. Celi et al., 2013; Turner and Engelbrecht, 2011; Vincent et al., 2012).

If the discrepancy of these data confirms an incomplete understanding of the processes controlling inositol phosphate retention, it also raises the crucial criticism of the extraction methods efficiency for subsequent organic P characterization (George et al., 2018). Extraction with a 0.25 M NaOH and 0.05 M ethylenediaminetetraacetic acid (EDTA) solution (Cade-Menun and Liu, 2014) is most commonly adopted. Organic P forms present in such extracts can be characterized using solution ^{31}P nuclear magnetic resonance (NMR) spectroscopy (Cade-Menun, 2005; Cade-Menun and Liu, 2014). This step has proven to be particularly difficult in subsurface layers of soils with low P content (Bünemann et al., 2008; Doolette et al., 2009; Möller et al., 2000). Doolette et al. (2009) verified the identification of ^{31}P NMR signals by spiking model organic P compounds (including inositol hexaphosphate) into NaOH–EDTA soil extracts. Although this approach improved the interpretation of ^{31}P NMR spectra by better addressing the attribution of signals to the

4

appropriate compounds, it did not verify if inositol phosphates were completely extracted, characterized and quantified.

Based on these considerations, we hypothesized that the abovementioned Fe oxides may differently contribute to inositol phosphates retention and stabilization in soil, according to their specific properties. To test this hypothesis, we studied i) the extent and mechanisms of *myo*-inositol hexaphosphate (InsP6) sorption on haematite, magnetite and maghemite; ii) the reversibility of the reaction as affected by pH and in the presence of complexing agents; iii) the efficiency of NaOH-EDTA on extraction of InsP6 once sorbed on the studied Fe oxides. For comparative purposes, we also studied these processes with Pi (monopotassium phosphate, KH_2PO_4) and with goethite.

We also carried out computational studies on the InsP6 molecule structure in order to better understand the adsorption mechanisms by identifying the conformation that best fits with the oxide surfaces. Previous hypotheses on InsP6 adsorption mechanism were indeed obtained by combining the mechanisms proposed resulting from Pi adsorption (Goldberg and Sposito, 1985; Parfitt and Atkinson, 1976; Sposito, 1984) and the Pi/InsP6 adsorption ratio (Celi and Barberis, 2004; Ognalaga et al., 1994; Yan et al., 2014; 2015). However, the tentative mechanism given did not consider the configuration of the InsP6 enantiomer and whether the distances among the different phosphate groups of the InsP6 molecule were compatible with the OH groups of the mineral surface.

Materials and methods

1. Synthesis and characterization of iron oxides

Goethite (Gt) was prepared as described by Schwertmann and Cornell (1991), by dissolving $Fe(NO_3)_3 \cdot 9H_2O$ in deionized water, rapidly adding 5 M KOH and stirring. The suspension was immediately diluted with deionized water and kept at 70°C for 60 h. The suspension was then centrifuged, washed with deionized water and freeze-dried.

Haematite (Hm) was prepared by dissolving $Fe(NO_3)_3 \cdot 9(H_2O)$ in HNO_3 previously heated at 98°C (Schwertmann and Cornell, 1991). The suspension was kept as such for 7 days at 98 °C, then centrifuged, dialyzed and freeze-dried.

Magnetite (Mt) was obtained by dissolving 4.2 g of $Fe(SO_4) \cdot 7(H_2O)$ and 9.2 g of $Fe(NO_3)_3 \cdot 9(H_2O)$ in 100 ml of deionized water under N_2 flux. The solution was brought to 90°C and then basified with NH_4OH and sequentially diluted with deionized water. The suspension was kept at 90°C for 30 min under continuous stirring and subsequently cooled to room temperature. The magnetic powder was separated from the solution using a laboratory magnet and washed with deionized water until it resulted salt-free before freeze-drying.

Maghemite (Mh) was prepared as magnetite but, after stirring for 30 min, the suspension was brought to pH 3 with 0.1 M HCl, heated to 100°C for 2-3 hours and then cooled to room temperature. Maghemite was separated from the solution using a laboratory magnet, washed with deionized water until salt-free and then freeze-dried.

The four Fe oxides were characterized for their mineralogical and surface properties. X-ray diffraction (XRD) analyses were acquired at 25°C on air-dried oriented mounts (40 kV and 20 mA, Fe filtered Co-Kα radiation) with a Philips PW 1710 (PANalytical B.V., Almelo, The Netherlands). The XRD patterns were recorded in the range 2°-80°, with 0.02° steps at a scanning rate of 4 sec/step.

The content of total Fe was determined by atomic absorption spectrometry after extraction with Na dithionite-citrate-bicarbonate (Fe_{DCB}) (Mehra and Jackson, 1960), while the presence of poorly crystalline forms and/or the potential solubility of the oxide was estimated from Fe extraction with ammonium oxalate buffered at pH 3.0 (Fe_o) (Schwertmann, 1964).

The specific surface area (SSA) and porosity of the freeze-dried oxides were measured by N_2 adsorption/desorption isotherms at 77 K (Carlo Erba Sorptomatic 1900, Rodano, Italy) after 24 h of out-gassing at 313 K under vacuum ($<10^{-4}$ kPa). The SSA was calculated by applying the Brunaumer-Emmet-Teller

(BET) equation (Gregg and Sing, 1982). The mesopore (d=2-50 nm) surface was derived from the adsorption branch of the isotherms using the Barret-Joyner-Halenda model (Barrett et al., 1951). The micropore (d<2 nm) surface was calculated as the difference between the total SSA and the mesopore surface.

In order to determine the zeta potential, 20 mg of each oxide were dispersed in 0.005 M KCl and shaken for 24 h, then aliquots of 2.5 ml from each suspension were adjusted to pH values between 3 and 10 with HCl or KOH, and 0.005M KCl was added up to a final volume of 10 ml. After 24 hours of shaking the pH was measured electrometrically, while the electrophoretic mobility was determined by Laser Doppler Velocimetry coupled with Photon Correlation Spectroscopy, by using LVD-PCS DELSA 400 spectrometer (Beckman, Coulter Inc., Canada), equipped with a 5 mW He-Ne laser (632.8 nm). The electrophoretic mobility was then converted to the zeta potential (ζ) using the Smoluchowski equation (Hunter, 1988).

2. *Phosphates and computational studies*

The P compounds in this study were purchased from Sigma Aldrich. Solutions of InsP6 were prepared in deionized water and refrigerated at 4°C. The hydrolysis of organic phosphates in stock solutions was monitored by measuring the phosphate concentration in solution before each use.

For the computational calculations, the two InsP6 chair conformations (1-axial/5-equatorial and 5-axial/1-equatorial) were considered, as reported in Barrientos and Murthy (1996). The two structures were drawn with the use of the software GaussView 5.0.9 (Gaussian Inc., Wallingford, CT 06492 USA) then their geometry was investigated at the Hartree-Fock (HF) level of theory employing the 3-21G basis set, with Gaussian ® 09W software (Gaussian Inc., Wallingford, CT 06492 USA). The distances among the P and oxygen (O) atoms belonging to the six phosphate groups were then measured for the two conformers, with the help of Moldraw software (Ugliengo et al., 1993; http://www.moldraw.unito.it).

3. *Adsorption isotherms*

Prior to adsorption experiments, Gt, Hm, Mt and Mh were suspended in 0.01 M KCl at pH 4.5 for hydrating adsorption sites. Then 5.0 ml of each suspension containing 30 mg of oxide were added to 5.0 ml solutions with different amounts of InsP6 or Pi at pH 4.5. The suspensions were shaken in the dark for 24 h at 25°C and

Gt and Hm centrifuged at 3000 rpm for 15 min, while Mt and Mg suspensions were separated with a laboratory magnet. All supernatants were filtered through a 0.20 µm Millipore membrane.

Solution phosphate concentrations were determined on the filtered solutions as described by Ohno and Zibilske (1991), while InsP6 was hydrolyzed to inorganic phosphate by an acidic digestion, before colorimetric determination (Martin et al., 1999). Standards samples were also run to determine the recovery of InsP6 by this method.

The amount of adsorbed P in µmol P m^{-2} was determined by the following equation:

$$Q_a = 1 \cdot 10^{-6} \cdot [(C_0 - C_e) \cdot V]/(m \cdot SSA) \qquad \text{Eq. 1}$$

where C_0 is the initial concentration, C_e is the residual concentration [mol l^{-1}], V is the solution volume [l], m is the mass of the adsorbent [g] and SSA is its specific surface area [m^2 g^{-1}].

All experiments were performed in triplicate. Blank samples were run for each experiment to ensure that no adsorption to the containers had occurred.

Zeta potential (ζ) was measured on the samples after InsP6 or Pi interaction, by conveniently diluting 50 µl of each suspension with 3 ml of its own supernatant.

4. Effect of pH and complexing agents on the reaction reversibility

The reversibility of adsorption was checked on all Fe oxides saturated at 50 and 100% with InsP6 or Pi, obtained by estimating the maximum adsorption capacity through isotherms, as described before. After centrifugation and decantation of the supernatants, the samples were weighed to determine the amount of entrained solution. Then, 10 ml of 0.01 M KCl at pH 3.5, 4.5, 7.5 or 8.5 were added to the residues and the suspensions were shaken in the dark for 24 h at 25°C and then centrifuged; the supernatants were separated from the residues and filtered at 0.2 µm. The amount of P released from the Fe oxides was determined by measuring the P concentration in the supernatant and correcting it for the entrained P amount determined previously. For the samples saturated with InsP6, both released phosphate, derived from chemical hydrolysis

of InsP6, and desorbed InsP6 were determined by analysing P before and after acid digestion. No hydrolysis of InsP6 was detected during the desorption experiments.

The extractability of InsP6 or Pi from Fe oxides was also tested with 0.005 M sodium citrate (pH 8.3), performing the same procedure used for KCl desorption at different pHs. Dissolved Fe was measured in the supernatant for all experiments, by atomic absorption spectrometry. All experiments were run in triplicate and standard deviations were calculated.

5. *Efficiency of NaOH-EDTA extraction*

Another series of InsP6− and Pi−Fe oxide complexes at 50 and 100% of P saturation was prepared to evaluate the efficiency of NaOH-EDTA extraction. In this case, 30 mg of each system were extracted with 10 ml of 0.25 M NaOH + 0.05 M EDTA (Cade-Menun, 2005). The suspensions were shaken for 16 h, centrifuged and the supernatant analysed for determining P concentration. All experiments were run in triplicate and standard deviations were calculated.

Results

1. *Fe oxide characteristics*

The identity of the four synthesized Fe oxides was confirmed by their XRD patterns (Fig. 1). Crystalline goethite was identified by the sharp peak at 0.419 nm, corresponding to (110) reflection. The peaks at d-spacing of 0.366, 0.268 and 0.251 nm corresponding to (012), (104) and (110) reflections of haematite, respectively, confirmed the synthesis of well crystallized haematite (Cornell and Schwertmann, 1996), with few goethite impurities (peaks at d-spacing of 0.419 nm and 0.244 nm). Magnetite and maghemite patterns corresponded to those identified by Magnacca et al. (2014) and Serna and Morales (2004), respectively. The diffraction patterns of these two minerals were almost identical, with a very small shift towards higher angles of (313) and (400) reflections of maghemite, as indicated by Cornell and Schwertmann (1996).

The main surface properties of the Fe oxides are reported in Table 1. The specific surface area of Hm (46.8 m^2g^{-1}) was comparable with that of Gt (40.2 m^2g^{-1}) and much lower than that of Mt and Mh (92.3 and 115

m^{2}g^{-1}, respectively). All the N$_2$ adsorption isotherms were typical of mesoporous solids, with average pore diameter around 0.8 µm (not shown). The well crystallized structure of each mineral shown by XRD patterns was confirmed by a very low Fe$_O$/Fe$_{DCB}$ ratio for Gt and Hm, while it increased to around 0.6 for the magnetic oxides, which are quite soluble in oxalate (Walker, 1983). The point of zero charge was at pH 7.0 for Hm and Mh and at pH 8.0 for Gt and Mt, respectively (Table 1).

2. *Computational results*

The optimized geometries of the two InsP6 conformations and the distances among O and P atoms of the six phosphate groups are shown in Fig. 2 and Table 2. The sterically unhindered 1-axial/5-equatorial conformer (Fig. 2a) was obtained by positioning the phosphate group bound to C2 in axial position and the other five in equatorial position, oriented on the same molecular planes of the inositol moiety. In this conformation, the distances between O atoms of contiguous phosphate groups were in the 0.299-0.363 nm range but increased to more than 0.699 nm between the O atoms of the 2 and 4, 3 and 5, 4 and 6 non-contiguous groups. The distances among 3, 4, 5 and 6 P atoms were in the 0.424-0.455 nm range, while the distances between 2 and 4, 3 and 5, 6 and 4 P atoms were above 0.659 nm. Conversely, the sterically-hindered 5-axial/1-equatorial conformer (Fig. 2b) presented the phosphate group in C2 equatorial and the other five phosphate groups in axial position. The axial 4 and 6 phosphate groups were oriented in a plane opposite to the other four [1, 3, 5 (axial) and 2 (equatorial)], with respect to the molecular plane of the inositol moiety. In this case, the distances between the O atoms of contiguous and non–contiguous 1, 2, 3, and 5 phosphate groups were in the 0.32-0.38 nm range while the distances between the corresponding P atoms were in the 0.434-0.464 nm range. The distances among the O and P atoms of these groups and the ones oriented in the opposite plane were obviously higher (> 0.566 and > 0.586 nm, respectively).

3. *Adsorption isotherms*

The adsorption isotherms of InsP6 and Pi on Gt, Hm, Mt and Mh are shown in Fig. 3. The adsorption of InsP6 and Pi on Gt was adequately described by the Langmuir model, giving adsorption maxima of 0.456 and 1.690 $\mu mol\ P\ m^{-2}$, respectively, with a higher K_L value (affinity constant for the Langmuir model) for Pi than InsP6 (Fig. 3a and Table 3). By contrast, Hm showed a lower P retention capacity, reaching a maximum adsorption extent of 0.349 and 0.803 $\mu mol\ P\ m^{-2}$ for InsP6 and Pi, respectively (Fig. 3b). On Mt and Mh, InsP6 did not reach a plateau even at high P concentrations (Fig. 3c, d), while showing an increasing adsorption up to ~ 0.900 $\mu mol\ P\ m^{-2}$. Conversely, Pi reached a plateau at 1.60 and 1.44 $\mu mol\ P\ m^{-2}$ for Mt and Mh respectively, showing, however, a low affinity for the mineral surfaces (Table 3). The Freundlich model better fit the experimental data of Mt and Mh compared with Langmuir model (Table 3).

As expected, the zeta potential (ζ) of the unreacted Gt was +40 mV at pH 4.5 (Table 1). The adsorption of InsP6 rapidly reversed the surface charge reaching -20 mV at C_e 0.0035 $mmol\ l^{-1}$, corresponding to only 24% of surface saturation and -50 mV at the highest concentrations (Fig. 4). Conversely, after Pi adsorption, Gt remained positive up to a Pi saturation of 60% and then reached a negative charge of -25 mV with the highest Pi additions (Fig. 4). For haematite, with an initial ζ of +33 mV, InsP6 adsorption already led to negative values with less than 10% of surface saturation, whereas Pi adsorption reversed the charge at 69% of Pi saturation, leading ζ down to -25 mV at the highest concentrations (Fig. 4). The zeta potential of Mt was +38 mV and the surface rapidly became negative after InsP6 adsorption, with less than 10% of InsP6 saturation, and reached values of -36 mV at the highest concentrations. Conversely, the zeta potential declined after Pi adsorption to 0 requiring more than 90% of saturation, although it reached quite highly negative values at the highest Pi concentrations (-33 mV, Fig. 4). In the case of maghemite, again 10% of InsP6 saturation was enough to reach a plateau at -33 mV. The zeta potential instead gradually declined from +30 mV to 0 mV with 65% of Pi saturation, but even at the highest Pi concentrations it did not reach highly negative values (-12 mV).

4. *Desorption of P forms and Fe extraction*

Desorption of InsP6 and Pi was carried out with 0.01 M KCl at different pHs from the four oxides previously saturated with the two adsorbates at 50 and 100% (Table 4). With InsP6, we obtained values of desorption close to zero or even negative (indicating a further re-adsorption of InsP6 entrained within the oxide particles, during the release experiment) at both 50 and 100% saturation. A greater extent of desorption occurred only from Gt and Hm, releasing however a small percentage of the adsorbed amount of P (≤6% at 100% saturation). Iron release was negligible except from InsP6−Mt complexes where amounts of Fe in the 0.10-4.16 mg Fe g^{-1} oxide range were found (Table 4).

Desorption of Pi from 50% saturated Pi-oxides systems was negligible from all oxides, except Mh, in the pH range 3.5-7.5 (Table 4). At pH 8.5 the release was more appreciable from all oxides, except Mt, remaining however under 2.5% of the adsorbed amount. From maghemite, the Pi released increased from 1.44 to 2.64% with increasing pH. When the Pi-oxides were 100% saturated, desorption was more pronounced and increased with increasing pH in all cases and reaching, at pH 8.5, values as high as 13.4 and 18.3 % of the adsorbed amount for Mt and Mh, respectively. Iron release was low in all cases, with values higher than 0.10 mg Fe g^{-1} oxide due to the acidic pHs (Table 5).

Using a competing anion such as citrate, P desorption was strongly related to the type of Fe oxide (Fig. 5). Citrate was not so efficient in competing with InsP6, although a larger amount of the adsorbate was extracted from Hm, Mt, and Mh with respect to Gt, from which no InsP6 was released (Fig. 5). At 100% of saturation, Hm released the highest percentage of InsP6, whereas Mt and Mh released amounts even lower than those at 50% saturation. Iron release occurred again only with Mt and Mh (Table 4). For Pi, the desorption with citrate was more efficient: Gt released only 5% of Pi at 50% saturation, while the other oxides released a larger amount of Pi, in the 25-54% range, following the order Hm < Mt < Mh (Fig. 5). The same trend occurred at 100% saturation, reaching 69% of Pi release with Mh. Release of Fe occurred only with Mt and Mh (Table 5).

5. Efficiency of NaOH-EDTA extraction

The NaOH-EDTA extractant showed a different performance depending on P type, P saturation level and type of Fe oxide (Fig. 6). With InsP6, the level of surface saturation did not affect so much the percentage of extraction, but surprisingly, the greatest extraction occurred with Gt at both 50% (24%) and 100% of saturation (38%). The extraction efficiency was lower with the other oxides, ranging from 16 (Mt) to 30% (Hm) from the totally saturated oxides. Iron release occurred from both saturated systems and with the greatest values observed again for Mt (Table 5). With Pi, we observed a great difference between the 50% saturated oxides, which released less than 5% of the adsorbed P, and the totally saturated surfaces, where the extracted Pi increased in the order Gt < Hm < Mt < Mh in the 38-85% range. Iron release showed an opposite trend with a higher release from the 50% saturated systems in the order Gt < Hm < Mh < Mt (Table 5).

Discussion

1. Adsorption extent and isotherms

Adsorption extent and isotherm shapes were quite different among the four Fe (hydr)oxides. The amount of Pi retained by Gt was in line with the data reported in the literature at the 0-0.5 mmol P l^{-1} C_e range (Celi et al., 1999; Ognalaga et al., 1994; Torrent et al., 1990 and references therein). In terms of moles, the amount of adsorbed InsP6 was four times less than Pi. Following the previously hypothesized mechanism (Celi et al., 1999; Ognalaga et al., 1994), InsP6 bonds to Gt by four of its six phosphate groups, while the other two remain free, facing the bulk solution. However, this was not compatible with the 1-axial/5-equatorial conformation typical of InsP6 in solution at pH < 9 (Bauman et al., 1999; Murthy, 2006 and references therein). In this conformation, the O atoms of non-contiguous 3, 5 and 3, 6 phosphate groups disposed on the same planes of the carbon moiety were indeed at larger distances than the singly coordinate -OH groups present on the (110) face of Gt, ranging between 0.290 and 0.490 nm (data not shown), in agreement with Barron and Torrent (1996). Thus, the adsorption reaction possibly requires a ring-ring interconversion from the 1-axial/5-equatorial form to a more sterically hindered 5-axial/1-equatorial conformation, where the distances between the O atoms of both contiguous and non-contiguous 1, 2, 3 and 5 phosphate groups were

13

in the 0.320-0.380 nm range. Although these distances exactly matched those of the singly coordinate -OH groups present on Gt surface and allowed for the interaction of four phosphate groups of InsP6, the molecular arrangement required energy for the conformational change (Murthy, 2006), accounting for the lower affinity of InsP6 for Gt with respect to Pi (K_L 2.6·10^3 l mmol^{-1} for InsP6 vs 5.1·10^4 l mmol^{-1} for Pi). On the other hand, the great negative charge of the newly-formed surface indicated not only the occurrence of the two phosphate groups facing the bulk solution and deprotonated at pH 4.5, but gave also indirect evidence of the creation of a strong inner-sphere complex inside the shear plane (Arai and Sparks, 2001).

Compared to Gt, Hm showed a lower capacity to retain Pi, due to the fact that the pairs of contiguous singly coordinated –OH groups, which are involved in the specific adsorption of phosphate, do not occur on all faces of haematite (Barron and Torrent, 1996). The amount of adsorbed InsP6 was, however, similar to that adsorbed on Gt. Based on the Pi/InsP6 ratio of 2:1 and on distances of the O atoms of contiguous phosphate groups in the 1-axial/5-equatorial conformation, the molecule was supposed to be bound to the oxide by only two of its phosphate groups (Giaveno et al., 2008; Yan et al., 2014). The Hm surface characteristics limited indeed the number of phosphate groups per molecule involved in the adsorption mechanism, allowing a greater number of InsP6 molecules (and thus of P moles) to be adsorbed per surface unit with respect to the available adsorption sites. These results were also confirmed by Yan et al. (2014) who demonstrated, by ATR-FTIR, the formation of complexes between inositol phosphate and a synthesized haematite, with fewer surface sites occupied by the organic molecule compared with Pi maximum adsorption. The larger number of P groups faced to the bulk solution did not lead to reach the highly negative charge observed with Gt. Xu et al. (2017) showed that, compared to Pi, InsP6 highly promoted the stability of haematite colloidal suspensions through both electrostatic and steric repulsive forces; however, it can form both inner and outer–sphere complexes with Hm, which may lead to a lower change of the particle surface charge (Arai and Sparks, 2001).

Magnetite showed a greater Pi retention capacity than Hm, with values similar to Gt, even though the crystal structure is composed by Fe^{2+}/Fe^{3+} in a stoichiometric ratio of 1:2 and adsorption is supposed to occur only through the Fe^{3+} octahedral sites. Zach-Maor et al. (2011) identified by X-ray Photoelectron Spectroscopy Pi

14

bonding to nano-sized magnetite particles predominantly through bidentate surface complexes. Daou et al. (2007) showed, through Mössbauer and ATR-FTIR, that Pi adsorption on magnetite occurred with formation of monoprotonated binuclear species. The similar Pi adsorption extent and mechanism on Gt and Mt, despite the different crystalline structure, should be related to the dominance of Fe^{3+} octahedral sites on the surface of Mt (Serna and Morales, 2004). However, precipitation processes could also contribute to surface retention, due to dissolution of Mt caused by phosphate and re-precipitation as Fe phosphates, which neutralize the surface charge up to 90% of P saturation. Only at the highest P sorption values was the surface indeed negatively charged, indicating that phosphates were not further neutralized by the dissolved Fe cations, and might be facing the bulk solution with one deprotonated -OH group. This was confirmed by the fact that up to 90% of P saturation, 1.0% of Fe contained in the Mt was present in the solution after adsorption, whereas only 0.04% was found at the greatest P concentrations (data not shown). On the other hand, this highlights that, at low concentrations, phosphate can cause a moderate dissolution of Mt, while at higher values the anion protects the oxide surface, as also stated by Daou et al. (2007). Dissolution of Mt provoked by anion adsorption was instead more pronounced with InsP6, whose retention progressively increased up to 0.974 µmol m^{-2}, reaching more than double the amount adsorbed by Gt and Hm. However, above these concentrations, sorption drastically decreased (data not shown), likely due to dissolution of Mt determined by the great complexing capacity of InsP6 (Celi and Barberis, 2006). Such effect was observed mostly in poorly crystalline Fe and Al oxides (Celi et al., 2003) and highlights the low stability of Mt (Cornell and Schwertmann, 1996). Despite the simultaneous occurrence of adsorption and precipitation processes, the Pi/InsP6 ratio of around 2 may indicate a stoichiometric reaction with two phosphate groups of InsP6 involved in the adsorption mechanism, without the requirement of conformational changes of the adsorbed molecule.

Maghemite retained slightly greater amounts of Pi than Mt: the larger surface area and the higher amount of Fe^{3+} ions in the crystalline structure of Mh compared to Mt (Serna and Morales, 2004) could favour Pi adsorption through a ligand exchange mechanism (Tuutijärvi et al., 2010). However, the lower affinity of Pi for the Mh surface as well as the deviation of experimental data from Langmuir model could suggest a greater

contribution of outer-sphere complexes to the retention of Pi by Mh. The ζ values, close to zero at the highest Pi concentrations, may furnish further evidence of formation of outer-sphere surface complexes with Pi (Tuutijärvi et al., 2010), which only partly entered inside the shear plane and moderately affected the particle surface charge (Arai and Sparks, 2001). The copresence of inner- and outer-sphere surface complexes may be accompanied by some precipitation on the newly-formed surfaces, as suggested by the isotherm shape, contributing to both the larger retention compared to Mt and to the weakly negative surface charge. The retention of InsP6 on Mh seemed to follow the same behaviour as on Mt, but in the former case, sorption continued to increase at the highest C_e concentrations. This may be related to the greater crystallinity of Mh, which gains ion ordering when obtained by Mt oxidation (Serna and Morales, 2004). Nevertheless, also for Mh, InsP6 retention might involve precipitation aside from adsorption, leading to a non-stoichiometric ratio (Pi/InsP6 ratio << 2). Conformational changes or constrains of the isomer are here ruled out, because apparently less than two P groups are involved in the mechanism.

2. *Desorption as a function of pH and effect of citrate*

The efficiency of KCl in desorbing Pi at different pHs was moderate (Table 4). It was always negligible from the 50% saturated P-Fe oxides systems, with slightly higher values for Mh. Conversely, desorption strongly differed among the four Fe oxides at 100% P saturation, revealing a large reversibility of the reaction, especially for Mt and Mh, with increasing pH. This highlights the low stability of the complexes formed by Pi with Mt and Mh. However, when InsP6 was involved in the adsorption process, P release was close to zero or even negative from both 50 and 100% saturated systems: the strength of InsP6 retention led even to negative values due to re-sorption phenomena of InsP6 entrained within oxide particles during adsorption. Only in the case of Hm, with a moderate Langmuir affinity constant, was a modest percentage of InsP6 released into the solution as a function of pH. The formation of an outer-sphere InsP6–Hm complex involving only two phosphate groups led to a weaker bond, easier to cleave with respect to Gt. However, also with Mt and especially Mh the desorption was negligible as observed for Gt: the formation of precipitates on the surface may protect the surface itself from sorbate release in the presence of indifferent electrolytes like Cl^-. Thus, besides the affinity of the two anions for the surface, the configuration of the P-mineral complex and

16

the formation of multiple site bindings, as well as the occurrence of multiple processes, play an important role in the reversibility of the bond and govern the adsorption/desorption equilibrium (Celi et al., 2003; Shang et al., 1996; Yan et al., 2014).

Citrate showed a greater capacity to extract the two P forms from the four oxides with respect to KCl at high pH. Pi release efficiency was in the order Gt << Hm < Mt < Mh reaching values as high as 70% of the adsorbed amount released from Mh complexes at 100% P saturation. The effect of citrate on InsP6 release was on the contrary not stronger than that of a diluted KCl solution in the case of Gt, in agreement with Martin et al. (2004). It was instead consistent in the case of Hm, Mt and Mh and increased up to 30% from fully P-saturated oxides. As expected, competition of citrate with P-containing compounds can induce their removal and increase the negative surface charge due to citrate adsorption on unsaturated surfaces (Lopez-Hernandez et al., 1986; Nagarajah et al., 1968; Violante et al., 1991). The lower effectiveness of citrate to remove InsP6 than Pi was reported to be due to its inability to detach all the P groups involved in the multiple P bonding with the oxide surface and to the high negative charge determined by InsP6 adsorption in a large pH range (Celi et al., 2001; Martin et al., 2004). However, as citrate can displace each phosphate group by interacting with the surface through its three carboxylic groups, it can effectively remove InsP6 from Hm, Mt and Mh to a larger extent, since only one or two phosphate groups of the inositol molecule are involved in the interaction with the surface of the oxides. Citrate could have also induced Fe^{3+} complexation, causing oxide dissolution (Jones et al., 1996; Miller et al., 1986), but this mechanism seemed to be effective with only Mt and Mh, leading to Fe^{3+} concentrations in the solution higher than 0.22% of the initial Fe amount (Table 5).

Regardless of the amount of InsP6 retained by Hm, Mh and Mt, the formed P-oxide complexes were therefore less stable and more subjected to the competing effect of citrate, with respect to Gt. This may contribute to decrease InsP6 retention in Fe rich soils, as observed in different environments (McDowell et al. 2007; Turner et al. 2007), thanks to a weaker bonding with the oxide and to a better efficiency of plant exudates to remove P from the solid phase. The larger availability of InsP6 in the soil solution may consequently favour phytase hydrolysis and InsP6 decrease, in agreement with Giaveno et al. (2010) who found that phytases were able

to partly hydrolyze InsP6 adsorbed on haematite-rich clays and not that adsorbed on goethite-rich clays (Giaveno et al., 2010).

3. *Efficiency of NaOH-EDTA extraction*

The 0.25 M NaOH + 0.05 M EDTA solution, the most common extractant used for subsequent ^{31}P-NMR characterization of P forms (Cade-Menun and Liu, 2014), showed different performances based on the type of Fe oxide and on the level of P saturation. The latter seemed to affect especially the extraction of inorganic phosphate, with a better efficiency when the surfaces were completely covered by Pi, in the order Gt < Hm < Mt < Mh. The large extractability of Pi from Mt is in agreement with Daou et al. (2007) who removed 90% of adsorbed phosphate from magnetite using 1 M NaOH. Tuutijärvi et al. (2012) also observed that increasing NaOH concentration from 0.5 M to 2 M caused the complete desorption of arsenate from maghemite. In this context, an increase of NaOH concentration may improve the extracting capacity, although the discrepancy among the different oxides could remain. When considering InsP6, the surprisingly larger extraction expressed with Gt may be related to a better capacity of EDTA to compete with its four carboxyl groups for the same number of phosphate groups involved in the InsP6–Gt binding mechanism. This might also occur with Hm, although to a lower extent. However, the efficiency of this mechanism seemed to be reduced when multiple processes characterize the retention of InsP6, such as on Mt and Mh, probably due to a lower capacity of the extractant to dissolve InsP6 salts and to break the bonds with the oxide surface. Based on the results obtained by Tuutijärvi et al. (2012), a modification of the extractant solution, increasing NaOH concentration, could lead to a better extraction. A number of authors also tried to narrow the solid to solution ratio (McLaren et al., 2015; Turner, 2008) but this does not seem to be beneficial if applied to our case, due to the rapid exhaustion of hydroxide and significant lowering of the final pH of the extract (Turner, 2008), although it may increase the concentration of P species in the extracts. The use of sequential extractants that can act on the different oxide forms could be more promising: a selective extraction with NaOH-EDTA and oxalic acid, as tested by Jørgensen et al. (2015), could favour the dissolution of Mh and Mt and the quantitative recovery of the adsorbed InsP6, but it requires further investigation.

Conclusions

The four crystalline Fe oxides showed a different capacity to retain inorganic and organic P in the form of InsP6, depending on the mineral surface properties and on the stability of the P–mineral complexes, which govern the extent and strength of adsorption. This in turn controlled the reversibility of the reaction and the capacity of the tested extractants to remove Pi and InsP6 from the solids surface.

Compared to goethite, haematite showed a lower capacity to retain not only Pi but also InsP6, accounting for the greater P availability and faster biocycling in soils that apparently should retain more P due to their higher degree of evolution and larger content in secondary Fe oxides. Maghemite and magnetite showed a greater InsP6 retention capacity, but their larger instability can make the complex more prone to P release and subjected to the competing effect of anions such as OH^- and citrate. This may contribute to decrease InsP6 accumulation in Fe rich soils as a consequence of a weaker bond of the molecule with the oxide surface, and thanks to a better efficiency of plant exudates to remove P from the solid phase.

Finally, our results confirm the crucial criticism of the efficiency of NaOH-EDTA extraction method while stressing the discrepancy in recovering different percentages of inorganic and organic P from the four oxides. Starting from synthetic models, we demonstrated that the recovery efficiency and the relative distribution between inorganic and organic P forms is a function of P saturation level and type of Fe oxides, making unique evidence that organic P characterization is still a crucial issue, not only linked to improvement and interpretation of ^{31}P-NMR spectra, but also related to the previous step of extraction.

References

Anderson, G., 1980. Assessing organic phosphorus in soils, in: Khasawneh, F.E., Sample, E.C., Kamprath, E.J. (Eds.), The role of phosphorus in agriculture. ASA-CSSA-SSSA, Madison, Wisconsin, USA, pp. 411–431.

Arai, Y., Sparks, D.L., 2001. ATR-FTIR spectroscopic investigation on phosphate adsorption mechanisms at the ferrihydrite-water interface. J. Colloid Interface Sci. 214 (2), 317-326.

Barrett, E.P., Joyner, L.G., Halenda, P.P., 1951. The determination of pore volume and area distribution in porous substances. I. Computations from nitrogen isotherms. J. Am. Chem. Soc. 73 (1), 373–380.

Barrientos, L.G., Murthy, P.N.N., 1996. Conformational studies of *myo*-inositol phosphates. Carbohydr. Res. 296, 39-54.

Barrón, V., Torrent, J., 1996. Surface hydroxyl configuration of various crystal faces of hematite and goethite. J. Colloid Interface Sci. 177 (2), 407-410.

Barros, N.F., Filho, R.M., Comerford, N.B., Barros, N.F., 2005. Phosphorus sorption, desorption and resorption by soils of the Brazillan Cerrado supporting eucalypt. Biomass Bioenerg. 28 (2), 229–236.

Bauman, A.T., Chateauneuf, G.M., Boyd, B.R., Brown, R.E., Murthy, P.N.N., 1999. Conformational inversion processes in phytic acid: NMR spectroscopic and molecular modelling studies. Thetrahedon Lett. 40 (24), 4489-4492.

Bowman, R.A., Moir, J.O., 1993. Basic EDTA as an extractant for soil organic phosphorus. Soil Sci. Soc. Am. J. 57 (6), 1516-1518.

Bünemann, E.K., Marschner, P., Smernik, R.J., Conyers, M., McNeill, A.M., 2008. Soil organic phosphorus and microbial community composition as affected by 26 years of different management strategies. Biol. Fertil. Soils 44, 717-726.

Cade-Menun, B.J., 2005. Characterizing phosphorus in environmental and agricultural samples by ^{31}P nuclear magnetic resonance spectroscopy. Talanta 66 (2), 359-371.

20

Cade-Menun, B., Liu, C.W., 2014. Solution phosphorus-31 nuclear magnetic resonance spectroscopy of soils from 2005 to 2013: a review of sample preparation and experimental parameters. Soil Sci. Soc. Am. J. 78, 19-37.

Celi, L., Lamacchia, S., Ajmone-Marsan, F., Barberis, E., 1999. Interaction of inositol hexaphosphate on clays: adsorption and charging phenomena. Soil Sci. 164 (8), 574-585.

Celi, L., Presta, M., Ajmone-Marsan, F., Barberis, E., 2001. Effects of pH and electrolytes on inositol hexaphosphate interaction with goethite. Soil Sci. Soc. Am. J. 65 (3), 753-760.

Celi, L., De Luca, G., Barberis, E., 2003. Effects of interaction of organic and inorganic P with ferrihydrite and kaolinite-iron oxide systems on iron release. Soil Sci. 168 (7), 479-488.

Celi, L., Barberis, E., 2004. Abiotic stabilization of organic phosphorus in the environment, in: Turner, B.L., Frossard, E., Baldwin, D.S. (Eds.), Organic phosphorus in the environment. CABI Publishing, Wallingford, UK, pp. 113-132.

Celi, L., Barberis, E., 2006. Abiotic reactions of inositol phosphates in soil, in: Turner, B.L., Richardson, A.E., Mullaney, E.J. (Eds.), Inositol phosphates: linking agriculture and the environment. CABI Publishing, Wallingford, UK, pp. 207-220.

Celi, L., Cerli, C., Turner, B.L., Santoni, S., Bonifacio, E., 2013. Biogeochemical cycling of soil phosphorus during natural revegetation of *Pinus sylvestris* on disused sand quarries in Northwestern Russia. Plant Soil 367 (1-2), 121-134.

Colombo, C., Barrón, V., Torrent, J., 1994. Phosphate adsorption and desorption in relation to morphology and crystal properties of synthetic haematites. Geochim. Cosmochim. Acta 58 (4), 1261-1269.

Cornell, R.M., Schwertmann, U., 1996. The Iron oxides: structure, properties, reactions, occurrence and uses. VCH Publishers, Weinheim, Germany.

Daou, T.J., Begin-Colin, S., Grenèche, J.M., Thomas, F., Derory, A., Bernhardt, P., Legaré, P., Pourroy, G., 2007. Phosphate adsorption properties of magnetite-based nanoparticles. Chem. Mater. 19 (18), 4494-4505.

Doolette, A.L., Smernik, R.J., Dougherty, W.J., 2009. Spiking improved solution phosphorus-31 nuclear magnetic resonance identification of soil phosphorus compounds. Soil Sci. Soc. Am. J. 73 (3), 919-927.

Geelhoed, J.S., Hiemstra, T., Van Riemsdijk, W.H., 1998. Competitive interaction between phosphate and citrate on goethite. Environ. Sci. Technol. 32 (14), 2119-2123.

Geelhoed, J.S., Van Riemsdijk, W.H., Findenegg, G.R., 1999. Simulation of the effect of citrate exudation from roots on the plant availability of phosphate adsorbed on goethite. Eur. J. Soil Sci. 50, 379-390.

George, T.S., Richardson, A.E., Smith, B.J., Hadobas, P.A., Simpson, R.J., 2005. Limitations to the potential of transgenic *Trifolium subterraneum* L. plants that exude phytase when grown in soils with a range of organic P content. Plant Soil 258, 263-274.

George, T.S., Giles, C.D., Menezes-Blackburn, D., Condron, L.M., Gama-Rodrigues, A.C., Jaisi, D., Lang, F., Neal, A.L., Stutter, M.I., Almeida, D.S., Bol, R., Cabugao, K.G., Celi, L., Cotner, J.B., Feng, G., Goll, D.S., Hallama, M., Krueger, J., Plassard, C., Rosling, A., Darch, T., Fraser, T., Giesler, R., Richardson, A.E., Tamburini, F., Shand, C.A., Lumsdon, D.G., Zhang, H., Blackwell, M.S.A., Wearing, C., Mezeli, M.M., Almås, Å.R., Audette, Y., Bertrand, I., Beyhaut, E., Boitt, G., Bradshaw, N., Brearley, C.A., Bruulsema, T.W., Ciais, P., Cozzolino, V., Duran, P.C., Mora, M.L., de Menezes, A.B., Dodd, R.J., Dunfield, K., Engl, C., Frazão, J.J., Garland, G., González Jiménez, J.L., Graca, J., Granger, S.J., Harrison, A.F., Heuck, C., Hou, E.Q., Johnes, P.J., Kaiser, K., Kjær, H.A., Klumpp, E., Lamb, A.L., Macintosh, K.A., Mackay, E.B., McGrath, J., McIntyre, C., McLaren, T., Mészáros, E., Missong, A., Mooshammer, M., Negrón, C.P., Nelson, L.A., Pfahler, V., Poblete-Grant, P., Randall, M., Seguel, A., Seth, K., Smith, A.C., Smits, M.M., Sobarzo, J.A., Spohn, M., Tawaraya, K., Tibbett, M., Voroney, P., Wallander, H., Wang, L., Wasaki, J., Haygarth, P.M., 2018. Organic phosphorus in the terrestrial environment: A perspective on the state of the art and future priorities. Plant Soil 427, 191-208.

Giaveno, C., Celi, L., Cessa, R.M.A., Prati, M., Bonifacio, E., Barberis, E., 2008. Interaction of organic phosphorus with clays extracted from oxisols. Soil Sci. 173 (10), 694-706.

Giaveno, C., Celi, L., Richardson, A.E., Simpson, R.J., Barberis, E., 2010. Interaction of phytases with minerals and availability of substrate affect the hydrolysis of inositol phosphates. Soil Biol. Biochem. 42 (3), 491–498.

Goldberg, S., Sposito, G., 1985. On the mechanism of specific phosphate adsorption by hydroxylated mineral surface: A review. Commun. Soil Sci. Plant Anal. 16, 801-821.

Gregg, S.J., Sing, K.S.W., 1982. Adsorption, surface area and porosity. 2nd ed. Academic Press, London.

Hunter, R.J., 1988. Zeta potential in colloid science. Principles and applications. Academic Press, London.

Jones, D.L., Darrah, P.R., Kochian, L.V., 1996. Critical evaluation of organic acid mediated iron dissolution in the rhizosphere and its potential role in root iron uptake. Plant Soil 180, 57-66.

Jørgensen, C., Turner, B.L., Reitzel, K., 2015. Identification of inositol hexakisphosphate binding sites in soils by selective extraction and solution ^{31}P NMR spectroscopy. Geoderma 257-258, 22-28.

Lopez-Hernandez, D., Siegert, G., Rodriguez, J.V., 1986. Competitive adsorption of phosphate with malate and oxalate by tropical soils. Soil Sci. Soc. Am. J. 50 (6), 1460-1462.

Magnacca, G., Allera, A., Montoneri, E., Celi, L., Benito, D.E., Gagliardi, L.G, Gonzales, M.C., Mártire, D.O., Carlos, L., 2014. Novel magnetite nanoparticles coated with waste-sourced biobased substances as sustainable and renewable adsorbing materials. ACS Sustainable Chem. Eng. 2 (6), 1518-1524.

Martin, M., Celi, L., Barberis, E., 1999. Determination of low concentrations of organic phosphorus in soil solution. Commun. Soil Sci. Plant Anal. 30 (13–14), 1909–1917.

Martin, M., Celi, L., Barberis, E., 2004. Desorption and plant availability of myo-inositol hexaphosphate adsorbed on goethite. Soil Sci. 169 (2), 115-124.

McDowell, R.W., Cade-Menun, B., Stewart, I., 2007. Organic phosphorus speciation and pedogenesis: analysis by solution ^{31}P nuclear magnetic resonance spectroscopy. Eur. J. Soil Sci. 58 (6), 1348-1357.

McKercher, R.B., Anderson, G., 1989. Organic phosphate sorption by neutral and basic soils. Commun. in Soil Sci. Plant Anal. 20 (7-8), 723-732.

McLaren, T.I., Smernik, R.J., McLaughlin, M.J., McBeath, T.M., Kirby, J.K., Simpson, R.J., Guppy, C.N., Doolette, A.L., Richardson, A.E., 2015. Complex forms of soil organic phosphorus–A major component of soil phosphorus. Environ. Sci. Technol. 49, 13238–13245.

Mehra, O.P., Jackson, M.L., 1960. Iron oxide removal from soils and clays by a dithionite-citrate system buffered with sodium bicarbonate. Clays Clay Miner. 7, 317-327.

Miller, W.P., Zelazny, L.W., Martens, D.C., 1986. Dissolution of synthetic crystalline and noncrystalline iron oxides by organic acids. Geoderma 37 (1), 1-13.

Möller, A., Kaiser, K., Amelung, W., Niamskul, C., Udomsri, S., Puthawong, M., Haumaier, L., Zech, W., 2000. Forms of organic C and P extracted from tropical soils as assessed by liquid-state ^{13}C- and ^{31}P-NMR spectroscopy. Aust. J. Soil Res. 38, 1017-1035.

Murthy, P.P.N., 2006. Identification of inositol phosphates by nuclear magnetic resonance spectroscopy: unravelling structural diversity, in: Turner, B.L., Richardson, A.E., Mullaney, E.J. (Eds.), Inositol phosphates: linking agriculture and the environment. CABI Publishing, Wallingford, UK, pp. 7-22.

Nagarajah, S., Posner, A.M., Quirk, J.P., 1968. Desorption of phosphate from kaolinite by citrate and bicarbonate. Soil Sci. Soc. Am. Proc. 32, 507-510.

Ognalaga, M., Frossard, E., Thomas, F., 1994. Glucose-1-phosphate and myo-inositol hexaphosphate adsorption mechanisms on goethite. Soil Sci. Soc. Am. J. 58 (2), 332-337.

Ohno, T., Zibilske, L.M., 1991. Determination of low concentration of phosphorus in soil extracts using malachite green. Soil Sci. Soc. Am. J. 55 (3), 892-895.

Parfitt, R.L., Atkinson, R.J., 1976. Phosphate adsorption on goethite (α-FeOOH). Nature 264, 740-742.

Santoro, V., Martin, M., Persson, P., Lerda, C., Said-Pullicino, D., Magnacca, G., Celi, L., 2019. Inorganic and organic P retention by coprecipitation during ferrous iron oxidation. Geoderma 348, 168-180.

Schaefer, C.E.G.R., Fabris, J.D., Ker, J.C., 2008. Minerals in the clay fraction of Brazilian Latosols (Oxisols): a review. Clay Miner. 43, 137–154.

Schwertmann, U., 1964. The differentiation of iron oxide in soils by a photochemical extraction with acid ammonium oxalate. Z. Pflanzenenähr. Düng. Bodenk. 105, 194-202.Schwertmann, U., Cornell, R.M., 1991. Iron oxides in the laboratory. Preparation and characterization. WILEY-VCH Verlag gmbH, Weinheim, Germany.

Serna, C.J., Morales, M.P., 2004. Maghemite (γ-Fe$_2$O$_3$): a versatile magnetic colloidal material, in: Matijević, E., Borkovec, M. (Eds.), Surface and colloid science. Surface and colloid science, vol 17. Springer, Boston, Massachusetts, pp. 27-81.

Shang, C., Caldwell, D.E., Stewart, J.W.B., Tiessen, H., Huang, P.M., 1996. Bioavailability of organic and inorganic phosphates adsorbed on short-range ordered aluminium precipitate. Microb. Ecol. 31, 29-39.

Sposito, G., 1984. The surface chemistry of soils. Oxford University Press, New York.

Torrent, J., Barron, V., Schwertmann, U., 1990. Phosphate adsorption and desorption by goethites differing in crystal morphology. Soil Sci. Soc. Am. J. 54, 1007-1012.

Turner B.L., 2007. Inositol phosphates in soil: amounts, forms and significance of the phosphorylated inositol stereoisomers. In: Turner B.L., Richardson A.E., Mullaney E.J., editors. Inositol phosphates: linking agriculture and the environment. CABI Publishing, Wallingford, UK, pp. 7-22.

Turner, B.L., Condron, L.M., Richardson, S.J., Peltzer, D.A., Allison, V.J., 2007. Soil organic phosphorus transformations during pedogenesis. Ecosystems 10 (7), 1166-1181.

Turner, B.J., 2008. Soil organic phosphorus in tropical forests: an assessment of the NaOH–EDTA extraction procedure for quantitative analysis by solution ^{31}P NMR spectroscopy. Eur. J. Soil Sci. 59, 453-466.

Turner, B.L., Engelbrecht, B.M.J., 2011. Soil organic phosphorus in lowland tropical rain forest. Biogeochemistry 103 (1), 297-315.

Tuutijärvi, T., Lu, J., Sillanpää, M., Chen, G., 2010. Adsorption mechanism of arsenate on crystal γ-Fe$_2$O$_3$ nanoparticles. J. Environ. Eng. 136 (9), 897-905.

Tuutijärvi, T., Repo, E., Vahala, R., Sillanpää, M., Chen, G., 2012. Effect of competing anions on arsenate adsorption onto maghemite nanoparticles. Chin. J. Chem. Eng. 20 (3), 505-514.

Ugliengo, P., Viterbo, D., Chiari, G., 1993. MOLDRAW: Molecular graphics on a personal computer. Z. Kristallogr. 207, 9-23.

Vincent, A.G., Schleucher, J., Gröbner, G., Vestergren, J., Persson, P., Jansson, M., Giesler, R., 2012. Changes in organic phosphorus composition in boreal forest humus soils: the role of iron and aluminium. Biogeochemistry 108 (1-3), 485-499.

Violante, A., Colombo, C., Buondonno, A., 1991. Competitive adsorption of phosphate and oxalate by aluminum oxides. Soil Sci. Soc. Am. J. 55 (1), 65-70.

Walker, A.L., 1983. The effects of magnetite on oxalate- and dithionite-extractable iron. Soil Sci. Soc. Am. J. 47 (5), 1022-1026.

Xu, C.Y., Li J.Y, Xu, R.K., Hong, Z.N., 2017. Sorption of organic phosphates and its effects on aggregation of hematite nanoparticles in monovalent and bivalent solutions. Environ. Sci. Pollut. Res. 24, 7197–7207.

Yan, Y.P., Liu Jr., F., Li, W., Liu, F., Feng, X.H., Sparks, D.L., 2014. Sorption and desorption characteristics of organic phosphates of different structures on aluminium (oxyhydr)oxides. Eur. J. Soil Sci. 65 (2), 308-317.

Yan, Y.P., Koopal, L.K., Liu, F., Huang, Q., Feng, X., 2015. Desorption of myo-inositol hexakisphopshate and

phosphate from goethite by different reagents. J. Plant Nutr. Soil Sci. 178 (6), 878-887.

Zach-Maor, A., Semiat, R., Shemer, H., 2011. Adsorption-desorption mechanism of phosphate by

immobilized nano-sized magnetite layer: Interface and bulk interactions. J. Colloid Interface Sci.
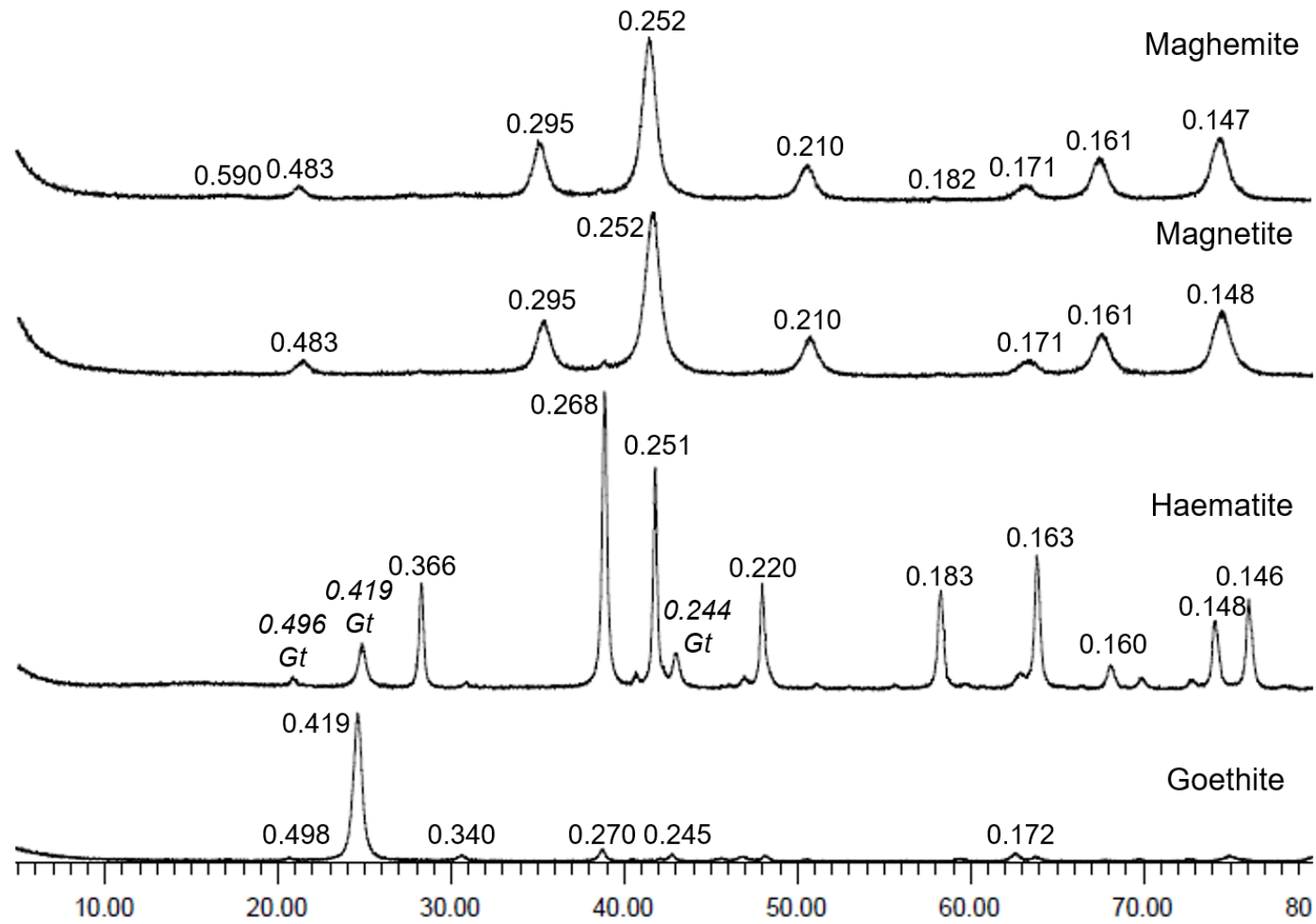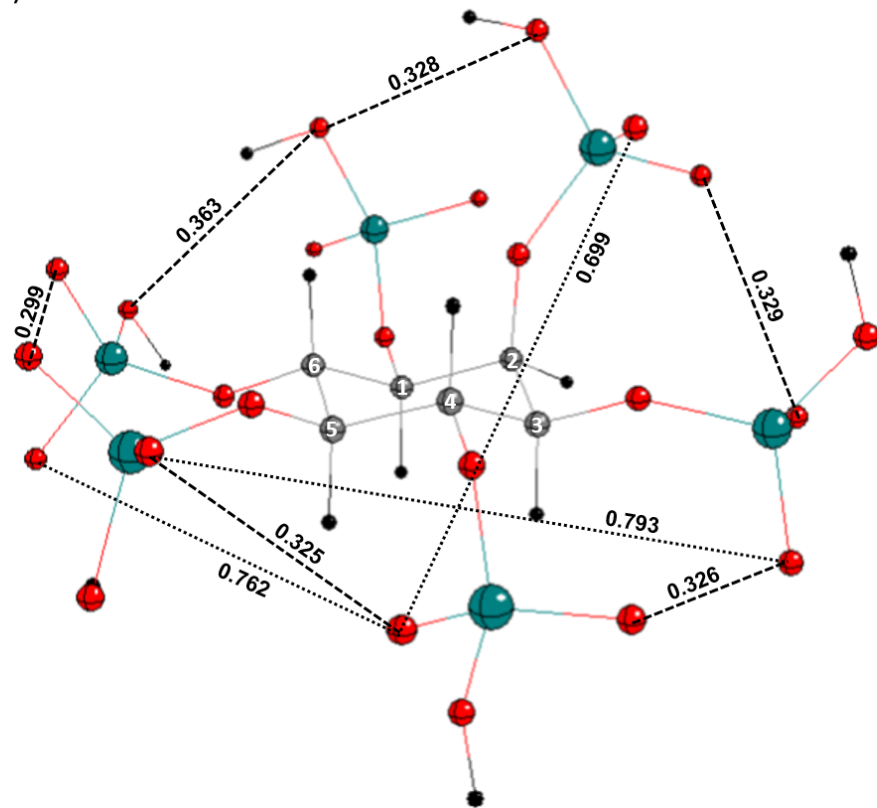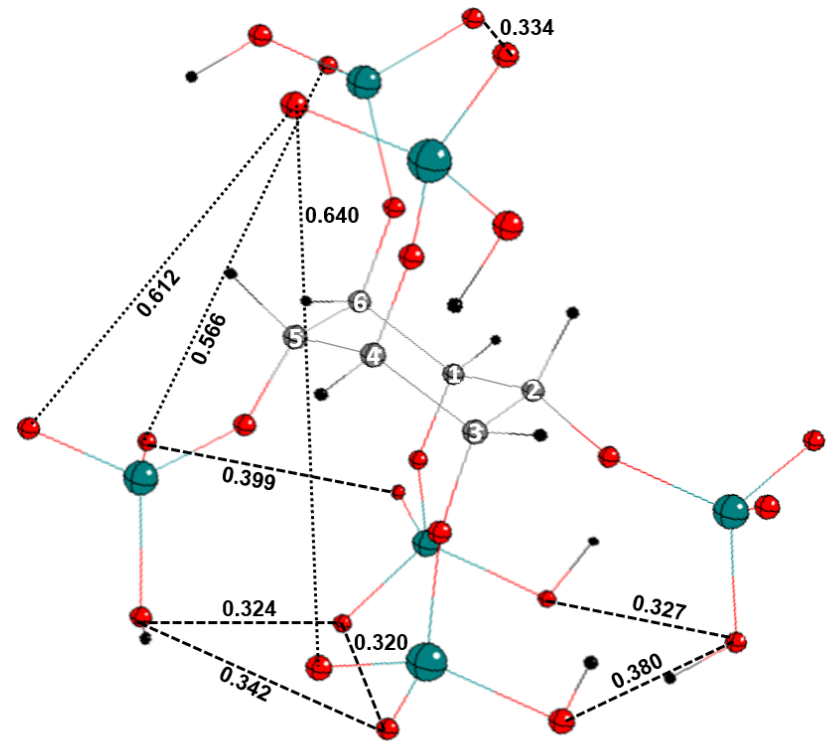
363, 608-614.

Figure 1

Figure 2
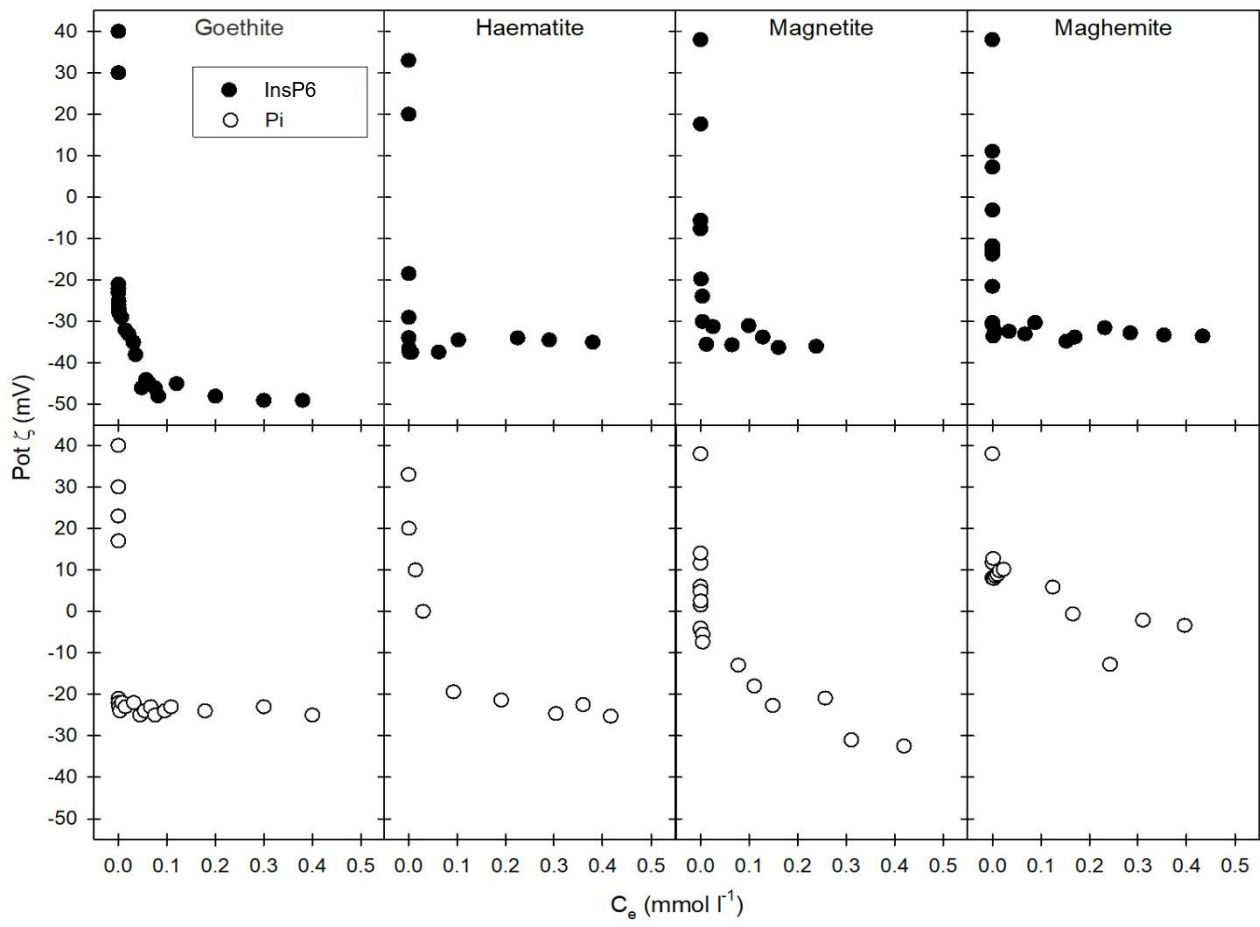

a)

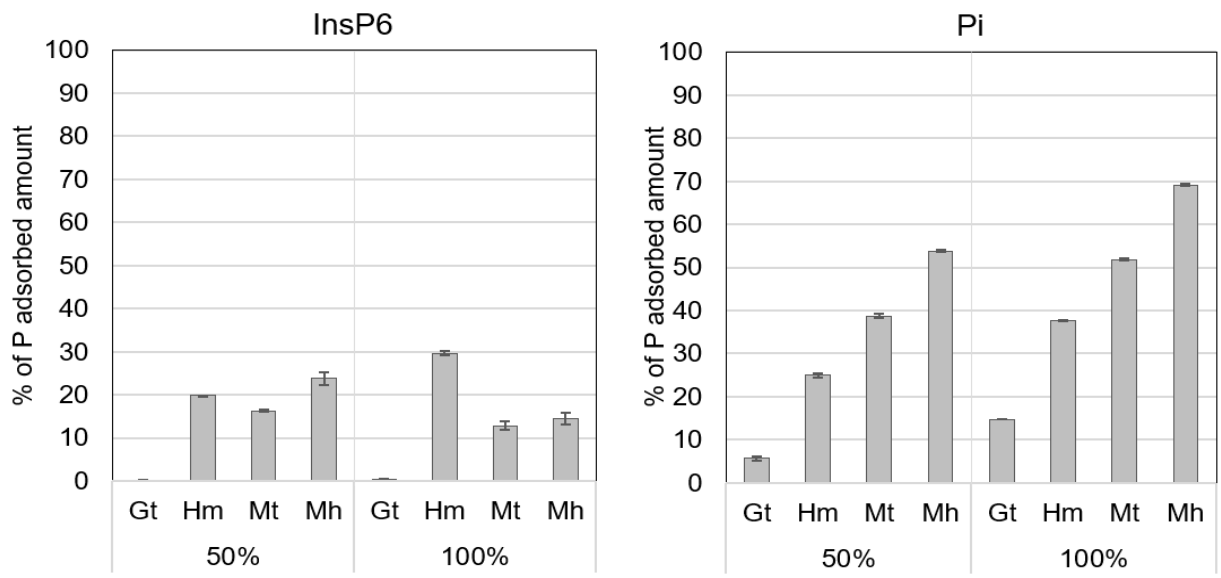b)

Figure 3
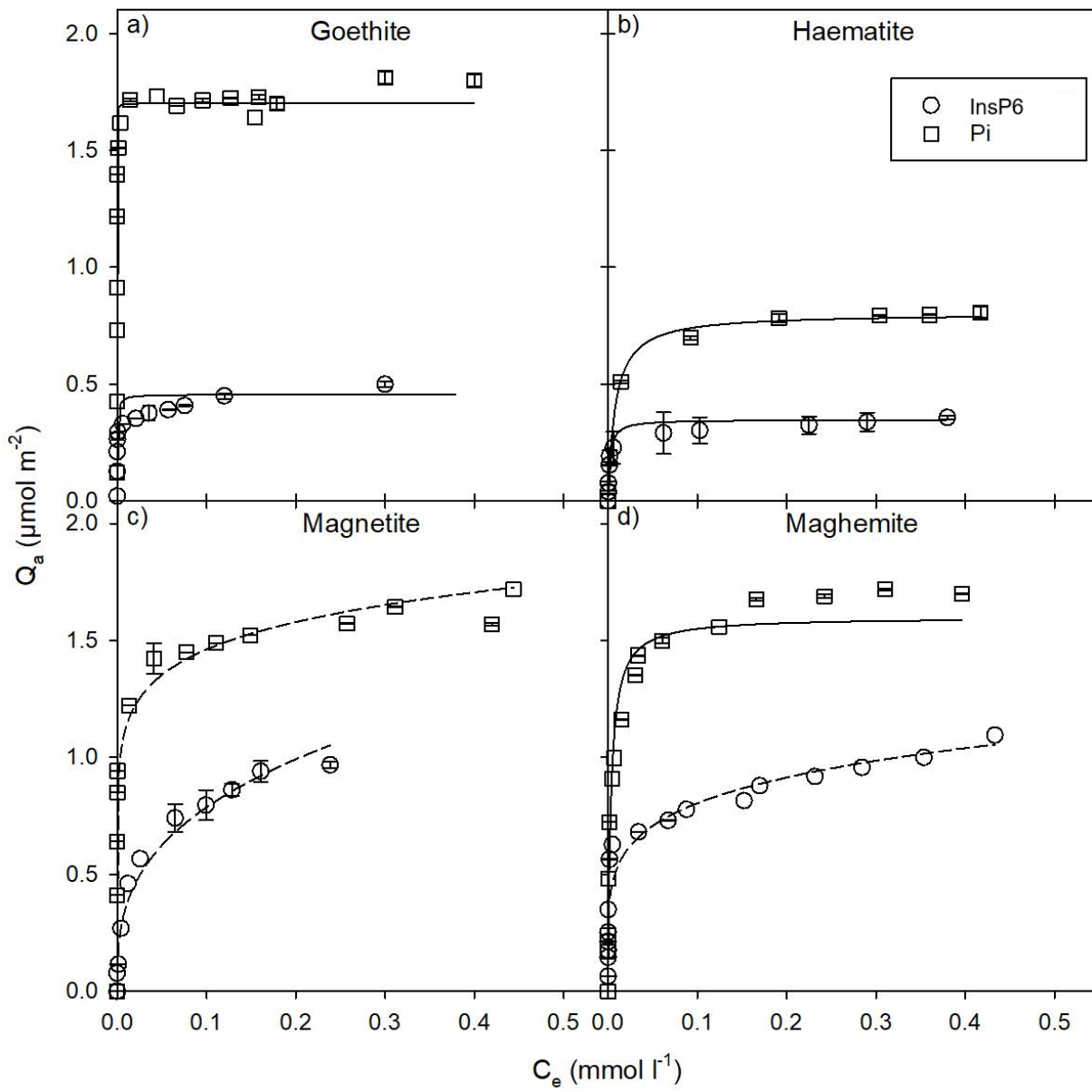
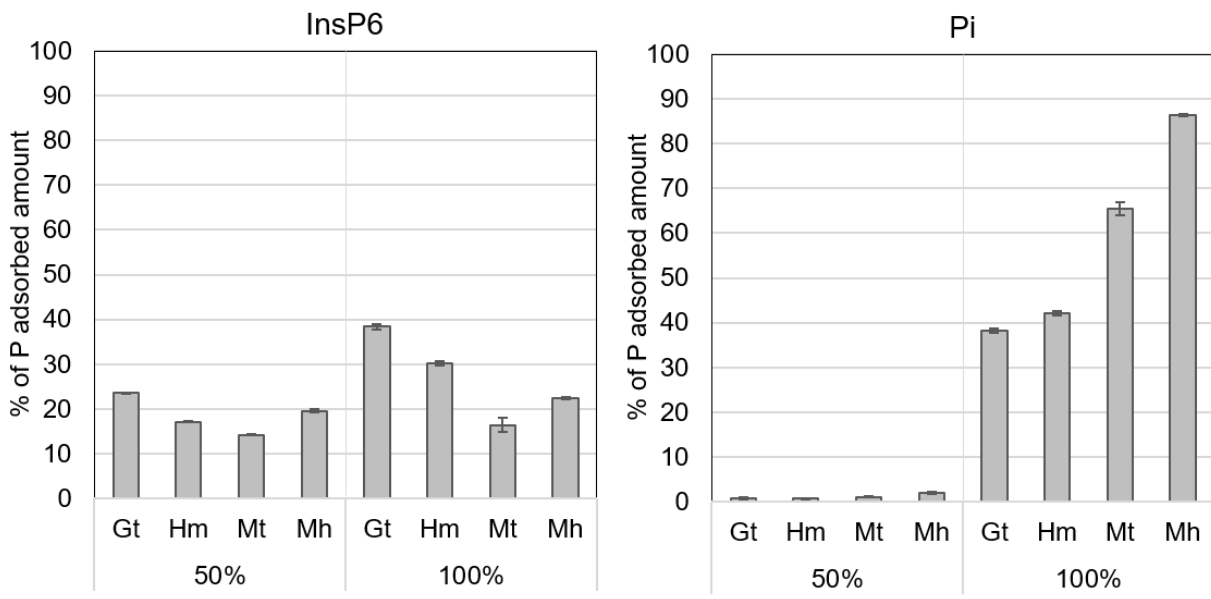**Figure 4**

Figure 5

Figure 6

Figure Captions

Figure 1. X-ray diffractograms of goethite, haematite, magnetite and maghemite. Labels represent d-spacing values expressed in nm. Gt, goethite.

Figure 2. Computational a) 1-axial/5-equatorial conformer and b) 5-axial/1-equatorial conformer of *myo*-inositol hexaphosphate (InsP6). Colors legend: black = hydrogen (H), grey = carbon (C), red = oxygen (O) and dark green = phosphorus (P). Lines legend: dashed lines = O bound to contiguous phosphate groups; dotted lines = O bound to non-contiguous phosphate groups.

Figure 3. Adsorption isotherms of *myo*-inositol hexaphosphate (InsP6) and inorganic phosphate (Pi) on a) goethite (Gt), b) haematite (Hm), c) magnetite (Mt) and d) maghemite (Mh) at pH 4.5. Experimental data were fitted with Langmuir (solid lines) or Freundlich (dashed lines) models. Q_a: amount of adsorbed P at equilibrium ($\mu mol\ m^{-2}$)$\dot{,}$ C_e: residual concentration ($mmol\ l^{-1}$). Values represent the mean of three replicates and error bars represent the standard error of the mean.

Figure 4. Variations of zeta potential (ζ) of complexes obtained with *myo*-inositol hexaphosphate (InsP6) or inorganic phosphate (Pi) and the four oxides as a function of the concentration of P at the sorption equilibrium concentration (C_e).

Figure 5. Na-citrate extraction of *myo*-inositol hexaphosphate (InsP6) and phosphate (Pi) adsorbed on goethite (Gt), haematite (Hm), magnetite (Mt) and maghemite (Mh), at 50 and 100% saturation. Values represent the mean of three replicates and error bars represent the standard error of the mean.

Figure 6. Extraction with NaOH-EDTA of *myo*-inositol hexaphosphate (InsP6) and phosphate (Pi) adsorbed on goethite (Gt), haematite (Hm), magnetite (Mt) and maghemite (Mh), at 50 and 100% saturation. Values represent the mean of three replicates and error bars represent the standard error of the mean.

Table 1. Specific surface area (SSA), total volume of pores (V_{tot}), ratio between amorphous Fe (extracted in Na oxalate) and crystalline Fe (extracted in Na dithionite–citrate–bicarbonate) (Fe_O/Fe_{DCB}), point of zero charge (PZC), and zeta potential at pH4.5 ($\zeta_{pH4.5}$) of goethite (Gt), haematite (Hm), magnetite (Mt) and maghemite (Mh).

Fe oxide	SSA	V_{tot}	Fe_O/Fe_{DCB}	PZC	$\zeta_{pH\,4.5}$
	$m^2 g^{-1}$	$cm^3\, g^{-1}$		mV	mV
Gt	40.2	0.28	0.001	8.0	+40
Hm	46.8	0.12	0.002	7.0	+33
Mt	92.3	0.24	0.640	8.0	+38
Mh	115	0.33	0.620	7.0	+30

Table 2. Computational geometric distances between oxygen (O) and phosphorus (P) atoms belonging to 1-axial/5-equatorial and 5-axial/1-equatorial conformers of *myo*-inositol hexaphosphate (InsP6). The O number (O_n-O_m) is referred to the P group to which it belongs. Only the shortest distance between the O atoms of two different phosphate groups was reported.

1-axial/5-equatorial conformer				5-axial/1-equatorial conformer			
O_n-O_m	Distance (nm)	P_n-P_m	Distance (nm)	O_n-O_m	Distance (nm)	P_n-P_m	Distance (nm)
O_1-O_2	0.328	P_1-P_2	0.413	O_1-O_2	0.327	P_1-P_2	0.471
O_2-O_3	0.329	P_2-P_3	0.418	O_2-O_3	0.380	P_2-P_3	0.445
O_3-O_4	0.326	P_3-P_4	0.455	O_3-O_4	0.640	P_3-P_4	0.603
O_4-O_5	0.325	P_4-P_5	0.441	O_4-O_5	0.612	P_4-P_5	0.645
O_5-O_6	0.299	P_5-P_6	0.424	O_5-O_6	0.566	P_5-P_6	0.586
O_6-O_1	0.363	P_6-P_1	0.427	O_5-O_1	0.324	P_5-P_1	0.434
O_2-O_4	0.699	P_2-P_4	0.659	O_1-O_3	0.320	P_1-P_3	0.460
O_3-O_5	0.793	P_3-P_5	0.770	O_3-O_5	0.342	P_1-P_5	0.464
O_6-O_4	0. 762	P_6-P_4	0.716	O_6-O_4	0.334	P_6-P_4	0.426

Table 3. Langmuir and Freundlich coefficients of adsorption isotherms of *myo*-inositol hexaphosphate (InsP6) and phosphate (Pi) on goethite (Gt), haematite (Hm), magnetite (Mt) and maghemite (Mh).

	Langmuir $$Q_a = \frac{Q_{max} \cdot C_e \cdot K_L}{1 + K_L \cdot C_e}$$			Freundlich $$Q_a = K_f \cdot C_e^{\frac{1}{n}}$$		
	Q_{max} $\mu mol\ m^{-2}$	K_L $L\ mmol^{-1}$	R^2	K_f $\mu mol\ m^{-2}$	n	R^2
Gt-InsP6	0.456	$2.6 \cdot 10^3$	0.738	0.594	0.135	0.846
Gt-Pi	1.690	$5.1 \cdot 10^4$	0.750	1.871	0.034	0.663
Hm-InsP6	0.349	$4.8 \cdot 10^2$	0.956	0.429	0.184	0.919
Hm-Pi	0.803	$1.3 \cdot 10^2$	0.902	0.873	0.120	0.966
Mt-InsP6	0.974	$0.7 \cdot 10^2$	0.981	1.232	0.185	0.924
Mt-Pi	1.443	$7.7 \cdot 10^3$	0.894	2.199	0.166	0.961
Mh-InsP6	0.861	$1.6 \cdot 10^3$	0.836	1.670	0.335	0.973
Mh-Pi	1.600	$3.1 \cdot 10^2$	0.913	1.890	0.112	0.935

Table 4. Desorption of *myo*-inositol hexaphosphate (InsP6) and phosphate (Pi) sorbed on goethite (Gt), haematite (Hm), magnetite (Mt) and maghemite (Mh) at 50 and 100% surface saturation in 0.01 M KCl at pH 3.5, 4.5, 7.5 and 8.5. Values are expressed as the percentage of the adsorbed amount (%) and were means of three replicates (± standard error).

	P type	InsP6				Pi			
	pH	3.5	4.5	7.5	8.5	3.5	4.5	7.5	8.5
50% saturation	Gt	-0.01 ± 0.03	-0.02 ± 0.01	0.03 ± 0.01	0.05 ± 0.01	0.03 ± 0.02	0.60 ± 0.26	0.20 ± 0.43	1.10 ± 0.45
	Hm	0.00 ± 0.01	0.01 ± 0.01	0.01 ± 0.02	0.04 ± 0.02	0.06 ± 0.06	1.03 ± 0.40	1.13 ± 0.21	2.30 ± 0.43
	Mt	-0.13 ± 0.07	-0.02 ± 0.06	0.02 ± 0.01	0.01 ± 0.04	0.35 ± 0.12	0.35 ± 0.06	0.42 ± 0.19	0.03 ± 0.03
	Mh	-0.11 ± 0.06	-0.04 ± 0.07	-0.02 ± 0.18	-0.40 ± 0.33	1.44 ± 0.13	2.05 ± 0.12	2.64 ± 0.49	1.48 ± 0.05
100% saturation	Gt	0.01 ± 0.01	0.53 ± 0.06	1.51 ± 0.02	1.03 ± 0.16	1.40 ± 0.06	8.80 ± 0.12	9.31 ± 0.25	8.32 ± 0.34
	Hm	0.07 ± 0.03	3.40 ± 0.02	4.40 ± 0.01	6.04 ± 0.07	0.05 ± 0.05	7.11 ± 0.24	8.23 ± 0.12	8.10 ± 0.25
	Mt	-0.59 ± 0.13	-0.25 ± 0.05	-0.19 ± 0.20	-0.12 ± 0.15	0.56 ± 0.19	7.74 ± 0.18	10.3 ± 0.12	13.4 ± 0.50
	Mh	-0.21 ± 0.08	0.16 ± 0.08	0.18 ± 0.17	0.37 ± 0.02	4.35 ± 0.04	6.81 ± 0.59	10.0 ± 0.25	18.3 ± 0.04

Table 5. Iron release [expressed as mg of released Fe with respect to the amount of Fe oxide (g)] from goethite (Gt), haematite (Hm), magnetite (Mt) and maghemite (Mh) saturated with *myo*-inositol hexaphosphate (InsP6) and phosphate (Pi) at 50 and 100%, following P desorption with 0.01 M KCl at pH 3.5, 4.5, 7.5 and 8.5; or P extraction with citrate and NaOH-EDTA.

	P type	InsP6						Pi					
	Desorbing/ extracting agent	pH 3.5	pH 4.5	pH 7.5	pH 8.5	Citrate	NaOH-EDTA	pH 3.5	pH 4.5	pH 7.5	pH 8.5	Citrate	NaOH-EDTA
50% saturation	Gt	0.02	0.02	0.05	0.07	<0.01	0.40	<0.01	0.02	<0.01	<0.01	<0.01	0.59
	Hm	0.01	0.02	0.02	0.01	<0.01	0.23	<0.01	<0.01	0.02	<0.01	<0.01	0.93
	Mt	0.07	0.08	0.09	0.09	1.20	3.29	0.80	0.08	<0.01	0.01	1.43	4.29
	Mh	0.01	0.05	0.07	0.08	0.23	2.20	0.65	0.11	0.02	0.02	0.77	3.63
100% saturation	Gt	<0.01	0.02	0.06	0.03	<0.01	0.37	<0.01	0.02	<0.01	<0.01	<0.01	<0.01
	Hm	<0.01	<0.01	0.02	<0.01	<0.01	0.21	<0.01	<0.01	0.02	<0.01	<0.01	<0.01
	Mt	2.38	1.19	4.16	0.23	0.10	2.83	0.80	0.08	<0.01	<0.01	<0.01	<0.01
	Mh	0.02	0.02	0.03	0.07	0.22	2.26	0.64	0.10	0.06	0.02	0.77	<0.01